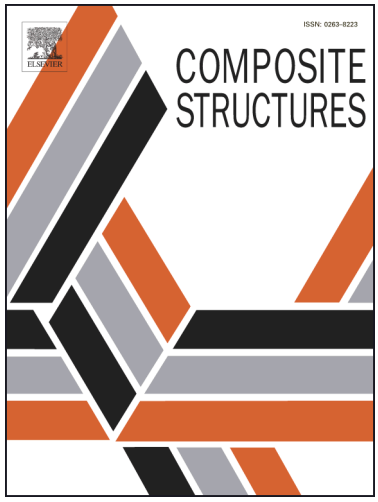

Quality assessment and damage detection in nanomodified adhesively-bonded composite joints using inkjet-printed interdigital sensors

Dimitrios G Bekas, Zahra Sharif-Khodaei, Dimitrios Baltzis, MH Ferri Aliabadi, Alkiviadis.S. Paipetis

PII: S0263-8223(18)34233-8
DOI: https://doi.org/10.1016/j.compstruct.2019.01.008
Reference: COST 10525

To appear in: *Composite Structures*

Received Date: 21 November 2018
Accepted Date: 2 January 2019

Please cite this article as: Bekas, D.G., Sharif-Khodaei, Z., Baltzis, D., Ferri Aliabadi, M., Paipetis, Alkiviadis.S., Quality assessment and damage detection in nanomodified adhesively-bonded composite joints using inkjet-printed interdigital sensors, *Composite Structures* (2019), doi: https://doi.org/10.1016/j.compstruct.2019.01.008

Quality assessment and damage detection in nanomodified adhesively-bonded composite joints using inkjet-printed interdigital sensors

Dimitrios G Bekas*[1], Zahra Sharif-Khodaei[1], Dimitrios Baltzis[2], M H Ferri Aliabadi[1] Alkiviadis. S. Paipetis[2]

[1] Structural Integrity and Health Monitoring Group, Department of Aeronautics, Imperial College London, South Kensington Campus, Exhibition Road, SW7 2AZ London, UK

2 Department of Materials Science & Engineering, University of Ioannina, Ioannina 45110, Greece

Abstract

In this work, the development of a planar interdigital capacitive sensor, directly onto the surface of a composite, for determining the initial quality of curing of bonded composite joints and assessing their long-term durability is presented. The sensor consisted of an interlocking comb-shaped array of silver electrodes and used to monitor the progress of cure of an adhesive resin and the subsequent damage state of the bond line in adhesively-bonded composite joints using impedance spectroscopy. The obtained results from the mechanical characterization indicated that the developed sensor did not affect the quality of the bondline while the added weight of the sensor is negligible. The curing process of the adhesive epoxy was successfully monitored while the ability of the sensor to assess the developed damage created by the mechanical loading was confirmed using transient infrared thermography.

Keywords: Bonded composite structures, damage detection, quality assessment, interdigital sensors, inkjet printing.

1 Introduction

Due to their increased fatigue resistance, high loading sustainability and low weight, adhesively bonded joints between composite structures, such as stiffened-skin or repairs, are excellent candidates to completely substitute mechanically fastened joints in military and civil aircraft [1-3]. However, deficient bonding quality processes and the absence of a reliable non-destructive evolution methodology for detecting poor bonding, have been a significant issue that results in the poor performance of these structures and limits their application to primary structures. Therefore, the development of Structural Health Monitoring (SHM) technologies that are able to provide accurate and reliable information on the bondline quality during manufacture

and the structural integrity of these structures during life time without adding any extra weight is of high importance.

Over the years, a variety of SHM methodologies have been proposed for the bondline inspection in adhesively bonded composite structures. Examples include Acoustic emission[4, 5], Lamb waves [6-10], Electro-mechanical impedance[11, 12], optical fibers [13, 14] and electrical-based methodologies [15-19]. The basis of all the aforementioned methods is continuously monitoring the response of the structure via an appropriate sensor or networks of sensors. To record the desired physical quantities such as displacement, force, vibrations or electrical resistance, sensors can be either surface mounted or embedded within the composite. In the case where the sensors are surface bonded, the operational conditions affect their performance and reliability. On the other hand, embedding of the sensors is usually favored since it offers physical protection for the sensor and does not affect the aerodynamics of the aircraft. However, embedding a foreign material (i.e. sensor, wiring, connectors) within the bondline of a lap joint will greatly affect its mechanical performance since it will create a discontinuity in the bondline and damage initiation sites. A possible solution to the aforementioned problem is using additive manufacturing.

In the last few years, innovative technologies and functional materials have been used to develop printed sensors for the SHM of composite structures. D. Zhao et al.[20] demonstrated an aerosol-jet printing technology for printing strain sensors inside composite structures that did not affect their mechanical performance. The printed sensors exhibited a reliable mean strain gauge factor which was comparable with that of a commercial strain gauge. The development of a strain sensor comprised of a highly durable ternary conductive nanocomposite made of polydimethylsiloxane (PDMS), carbon black (CB) and multi-walled carbon nanotubes (MWCNTs) was reported by F. Yin et al. [21]. The sensor showed an increased strain sensitivity, a high gauge factor and excellent durability over 10^5 stretching-releasing cycles. Although, printed sensors have been employed for the SHM of composite structures, there is currently no work related to the development of interdigital sensors directly onto the bondline of adhesively bonded composite-to-composite joint that will be able to assess both the bonding process and the integrity of the bondline during usage.

In this work, the development of a novel interdigital sensor for monitoring the curing and service damage in bonded composite-to-composite joints is presented. The sensors are directly inkjet-printed into the bondline and are comprised of an

interlocking comb-shaped array of silver electrodes and used to enable Impedance Spectroscopy measurements through the bondline. The inkjet-printed sensor was initially used to monitor and assess the curing process of the polymer adhesive during bonding. Afterwards, the Carbon Fiber Reinforced Polymer Composites (CFRP) joints were subjected to tensile step-loading and the initiation and propagation of damage within the bondline, was monitored by tracing changes in the impedance spectra. It should be highlighted that the interdigital sensor can be designed according to the dimensions of the bondline and selectively printed in key areas such as joints or repairs. To tailor the electrical response of the adhesive to higher frequencies of the impedance spectra and avoid the unwanted Electrode Polarization (EP) effect [22-24], the polymer adhesive was modified using multi-walled carbon nanotubes (MWCNTs). Infrared thermography was employed to validate the results obtained from the impedance spectroscopy while the fractured surfaces were studied under Scanning Electron Microscopy (SEM) so as to investigate the mechanisms of failure and gain an insight of the dispersion quality of the employed filler.

2 Inkjet-printed interdigital sensor

2.1 Design of the Printed sensor

The operating principle of a planar interdigital sensor is based on the rule of two parallel plate capacitors [25]. However, in this case, the electrodes open to provide one-sided access to the material under test. The electric field lines generated by the sensor penetrate the material under investigation to a curtain penetration depth (w). If the dielectric properties of the material change, e.g. by the presence of damage, the impedance of the sensor will also change. Therefore, the interdigital sensor acts as a capacitor in which the capacitive reactance becomes a function of system properties[25].

The design of the fingerlike periodic pattern of parallel in-plane electrodes is based on the area or volume that will be investigated. The penetration depth *w* above the interdigital electrodes is proportional to the spacing $\lambda/2$ between the centerlines of the planar electrodes. Where λ is the spatial wavelength or the wavelength of the spatial periodicity of the geometrical structure. In the case of the adhesively bonded joints, the penetration depth equals to the bondline thickness. Therefore, the interdigital sensor was purposely designed so that the electric field lines generated by the sensor will penetrate the entire adhesive thickness. A major advantage of the developed

methodology is that the developed sensor requires access only to one side of the structure and the signal's penetration depth can be controlled by modifying the sensor area, the number of fingers, and the spacing between them [25]. Therefore, the design of the sensor can be modified according to the dimensions of the bondline. Figure 1 depicts the geometrical characteristics of the interdigital sensor. In this case the total number of electrodes was 16 resulting in a total sensor length of L= 12.5mm while the width (S) of the sensor was selected at 12.5mm.

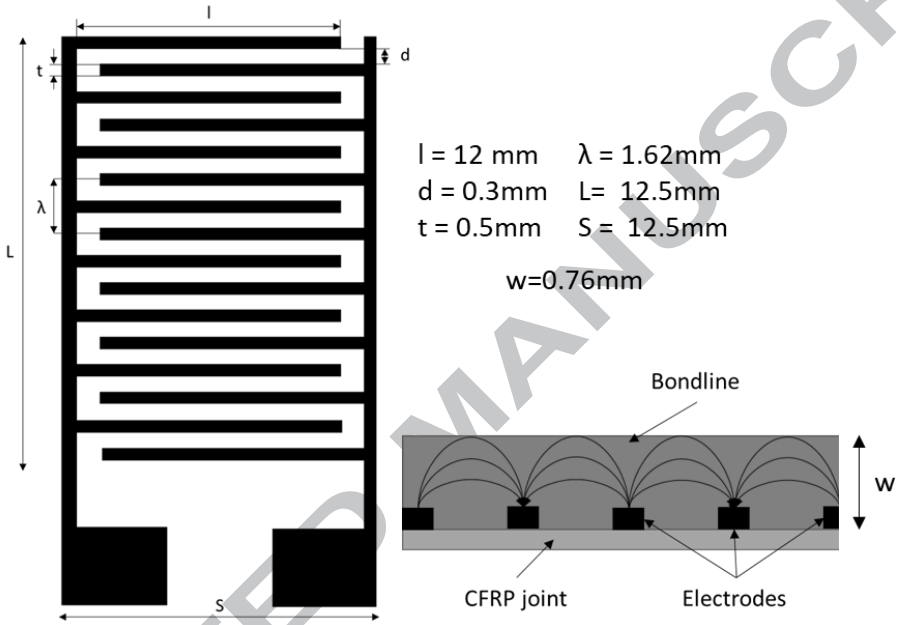

Figure 1 Geometrical characteristics of the developed sensor

2.2 Development of the printed sensor

Inkjet printing of the interdigital sensor onto the bondline was performed using a piezoelectric Dimatix DMP 2850 inkjet printer. A silver nanoparticle suspension supplied by Sigma-Aldrich was employed for the development of the interdigital electrodes. The silver ink contained 30-35 wt % of silver nanoparticles. The particle diameter was under 50 nm while the ink viscosity ranged from 10 to 18 mPa·s and the surface tension was between 35 and 40 $mN \cdot m^{-1}$. The printing frequency was set at 5 kHz while a modified waveform allowed a satisfactory droplet formation. The printer piezo voltage was selected at 20 V and the substrate temperature was selected at 60 °C. To increase the conductivity of the printed electrodes, 5 layers of silver-based ink were printed on top of each other. At the end of the printing process, sintering of the printed electrodes took place at 130^0C for 30min in a laboratory oven. At this stage any remaining traces of solvents were removed, and the particles fused into a cohesive

conductive line. It should be mentioned that the sintering temperature was lower than the glass transition temperature of the CFPR joints and did not introduce any thermal degradation to the specimens. Coaxial cables were attached to the sensor using silver conductive adhesive epoxy.

3 Adhesively bonded CFRP joints

3.1 Nanomodified epoxy adhesive

The Graphistrength Multi Wall CNTs supplied by ARKEMA, France were used for the modification of the epoxy adhesive. They were synthesized by Catalyzed Chemical Vapor Deposition (CCVD); the tube diameter ranged from 10 to 15 nm and the tube length was more than 500 nm. The nanotubes were in the form of agglomerated bundles with an average diameter of 400μm. As adhesive, the epoxy system Araldite LY 5052/Aradur 5052 was used. The mix ratio was 100: 38 by weight. Dispersion of 0.5% w/w MWCNTs in the host resin achieved using an ultrasonic mixer. CNTs and Araldite LY 5052 resin were carefully weighed and mixed together in a beaker. To avoid overheating of the polymer resin and introduction of defects on the CNTs surface, the temperature during the dispersion was kept at 25 ± 1^0C, using a cooling bath. CNTs were dispersed in the matrix using sonication for 4 h at 400W amplitude. It should be mentioned that the CNT content and the dispersion conditions were selected based on previous study [26].

3.2 CFRP joints

The CFRP specimens manufactured using 16 plies of aerospace grade unidirectional Hexply 914-TS-5-134 prepreg. The stacking sequence was $[0/45/-45/90]_{2s}$ while the composite final thickness was 2mm. At the end of the manufacturing process, single lap joint specimens were cut in the desired dimensions according ASTM D5868-01[27] using abrasive water jet. To enhance the adhesive strength, the bondline area of one of the composite joints was sanded using an air sand blaster. To ensure an electrical insulation between the conductive interdigital electrodes and the carbon fibers, a thin layer of epoxy resin, Araldite LY 5052/Aradur 5052, was screen coated onto the bondline area of the second composite joint. Adhesive bonding of the CFRP joints achieved using the nanomodified epoxy resin. The overlap area was 25mm×25mm and bondline thickness was 0.76mm as suggested by the standard [27]. To ensure this thickness, aluminum spacers were used during the bonding process.

Curing of the adhesive took place at 24^0C for 24h followed by a post-curing at 100^0C for 4h. At the end of the bonding process, the ends of the specimens were reinforced with end tabs. To investigate the effect of printing sensors on the shear strength of the bonded lap joints, a test campaign was carried out. Five lap joint specimens with and without the printed sensors were tested to assess the effect of sensor on the shear strength of the joints. Figure 2 depicts the printed sensor onto the bondline area along with the final single lap joint.

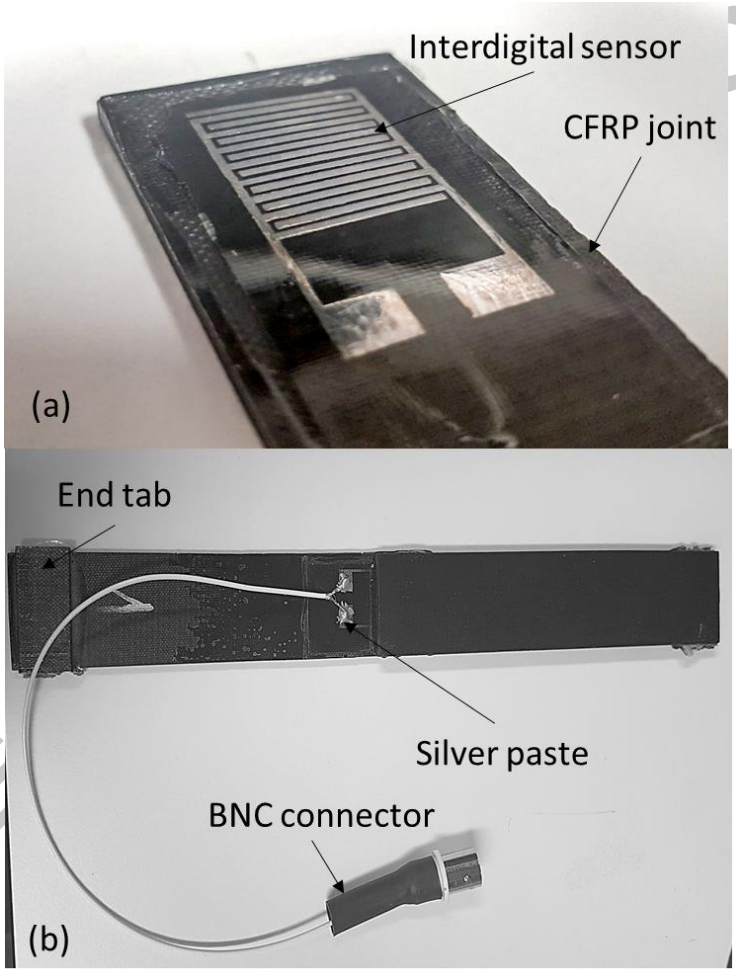

Figure 2 (a) Inkjet-printed sensor and (b) single-lap joint specimen

3.3 Effect of the sensor printing on the Maximum Shear Strength (MSS)

The effect of sensor development on the specimen's mechanical performance was evaluated through lap-shear tests. Figure 3 depicts representative load versus extension curves for the single lap joints with and without the printed sensor. As can be observed, the presence of the interdigital sensor had a negligible effect on the maximum failure load. In more detail, the failure load of the specimens without the

sensor was found at 5.54 ± 0.2kN while in the case of the single lap joints with printed sensor the failure load was 5.19 ± 0.3kN. It should be mentioned that the effect of modifying the adhesive epoxy using MWCNTs on the maximum shear strength has been extensively studied [28-31] and is therefore not investigated in this work.

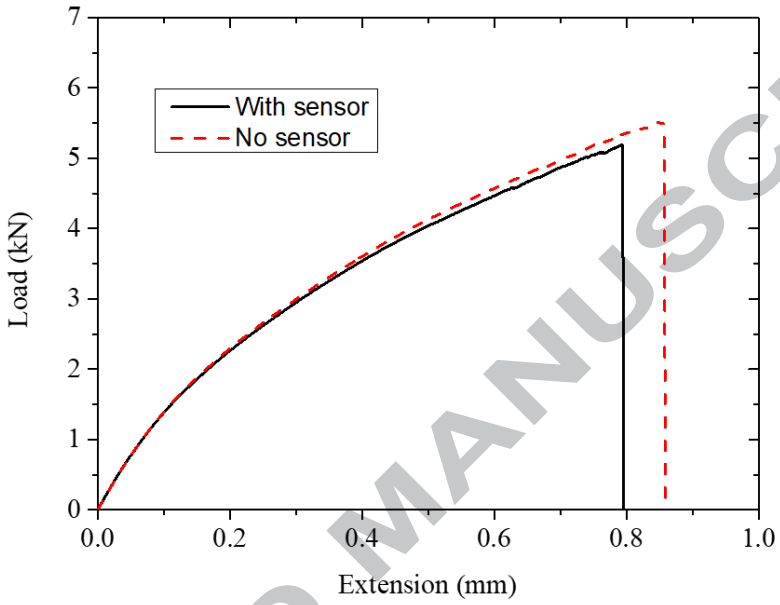

Figure 3 Load versus extension curves for the single lap joint with and without the printed sensor

The apparent maximum shear strength (MSS) of the lap joints was calculated according to ASTM [27] using equation (1):

$$\tau_{max} = \frac{L_{max}}{A} \quad (1)$$

where τ_{max} is the MSS, L_{max} is the maximum load and A is the bond area. Table 1 summarizes the calculated values of apparent shear strength for both cases.

Table 1 Maximum failure load and maximum apparent shear strength for the specimens with and without the printed sensor

Specimen	**L_{max} (kN)**	**τ_{max} (Mpa)**
No sensor	5.54 ± 0.25	8.86
With sensor	5.19 ± 0.30	8.19

Consistent data were obtained for both cases and a total reduction in maximum apparent shear strength of 7% was calculated. This reduction is not considered significant since it lies almost within the experimental scatter.

The remaining three single-bonded lap joints with the inkjet-printed sensor were subjected to step-loading tests of 20%, 40%, 60%, 80% and finally 100% of their maximum shear strength.

4 Cure monitoring

To access and evaluate the quality of the bondline, the process of cure of the CNT-modified adhesive epoxy was monitored using impedance spectroscopy. Impedance spectroscopy is a technique that has been extensively employed to investigate the processing characteristics, chemical structure or structural integrity of polymers and their composite materials by measuring their dielectric properties [32-36]. Therefore, phase transitions that take place during curing are expected to alter the dielectric profile of the adhesive. Impedance spectroscopy measurements were taken using a E4990A impedance analyzer supplied. The spectrometer applied a sinusoidal electrical excitation waveform of varying frequency, and the induced current waveform was recorded in real time. The excitation frequency ranged from 20 Hz to 3 MHz and the voltage amplitude was selected at 1 V. Four specimens were tested in total. To evaluate the ability of the inkjet-printed sensors to detect a defect during the bonding process, a small piece of Kapton film was placed on the bond area in one of the CFRP joints, partially covering the interdigital sensor.

The dielectric quantity that was recorded and studied, in order to monitor and evaluate the progress of cure, was the imaginary part of the impedance (Z’’max) [32, 37]. Z’’max can be directly related to the mobility of the charged species within the material and is highly affected by the phase transitions taking place within it, in this case the curing of the adhesive epoxy. Figure 4 depicts the evolution of Z’’max during the bonding process for four lap joints; one containing an artificial defect (specimen 4) and three without (Specimens 1, 2 and 3).

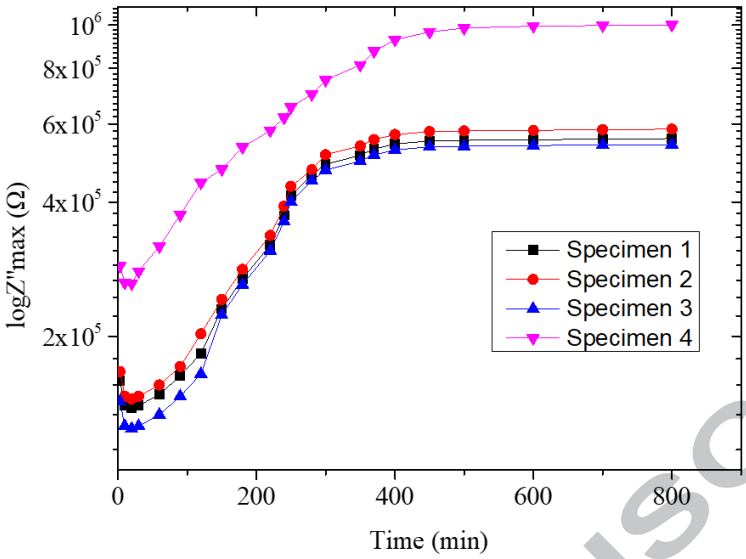

Figure 4 The evolution of the maximum of the imaginary part of the impedance (Z''max) during the bonding process of an undamaged and a damaged single lap joints

As can be observed from Figure 4, these curves exhibit similar trends, but the one corresponding to the damaged lap-joint shows higher values of Z''max. The difference in values between these two cases (defect and no defect) derives from the presence of Kapton film and entrapped air within the bondline. These two phases, that simulate defects during manufacturing, have different dielectric properties than the modified epoxy and greatly affect the dielectric profile of the interrogated system. Thus, by positioning the inkjet-printed sensor in different key areas of a composite structure, an evaluation of the bondline quality can be achieved by tracing the dielectric properties of the system. In both cases the Z''max values exhibited a small decrease at the early stage of curing, denoting an increase in ion mobility caused by the decrease in epoxy viscosity. This behavior can be attributed to a minor increase in epoxy's temperature due to the exothermic character of the curing reaction. Between 30 and 400 minutes, the gelation of the nanomodified epoxy resulted in a decrease in ionic mobility and was manifested as a monotonous increase in the Z''max curves. It should be mentioned that the gel time, as observed using the printed sensor, is in agreement with that reported in the epoxy datasheet. During the last stage of the bonding process the Z''max values reached a plateau, indicating the completion of cure.

5 Bondline Integrity Monitoring

To evaluate the ability of the proposed sensors to detect damage within the bondline, the single-lap joints were subjected to lap-shear tests. Loading-unloading lap-shear tests were performed using an Instron universal testing machine equipped with 50 kN load cell. The loading sequence involved incremental loading steps at extension control mode with constant extension rate of 1.5 mm/min. To determine the maximum shear strength, two specimens from each group were subjected to lap-shear tests until fracture according to ASTM D5868. The rest of the specimens were subjected to tensile step-loading of 20%, 40%, 60%, 80% and finally 100% of their maximum shear strength.

Impedance spectroscopy was employed in every step of the mechanical test, to achieve a correlation between the impedance data and the local material state changes associated with the irreversible damage that were accumulated during the tensile loading. For the impedance measurements the signal's excitation frequency varied from 20 Hz to 1 MHz and the voltage amplitude was selected at 1 V. Measurements were taken at ambient conditions with temperature and relative humidity of 23 ^{0}C and 50-60%, respectively.

Transient Infrared Thermography (IrT) was employed in-between the steps of the tensile test to validate the results from the impedance spectroscopy measurements and detect the initiation and propagation of damage within bondline. IrT measurements were conducted using a FLIR A615/25 IR camera. The camera is capable of acquiring full-frame 16-bit images at a frame rate of 50 Hz. As a heat source, an Ir-lamp was used. The recording duration of the IR camera was 30 s to monitor an entire period of heating and cooling. Phase thermographic images were obtained through Fast Fourier Transformation (FFT) of the acquired thermographs.

Figure 5 depicts the evolution of the impedance magnitude (log|Z|) and phase delay over the frequency spectrum (Bode plots) for all the stages of the step-loading lap shear tests. The first observation is that the Electrode polarization (EP) effect which impedes the impedance spectroscopy measurements for highly dielectric materials has been addressed via the incorporation of the MWCNTs. The presence of the highly conductive nanophase shifted the electrical response of the material under test towards higher frequencies resulting in a higher signal-to-noise ratio [34, 36].

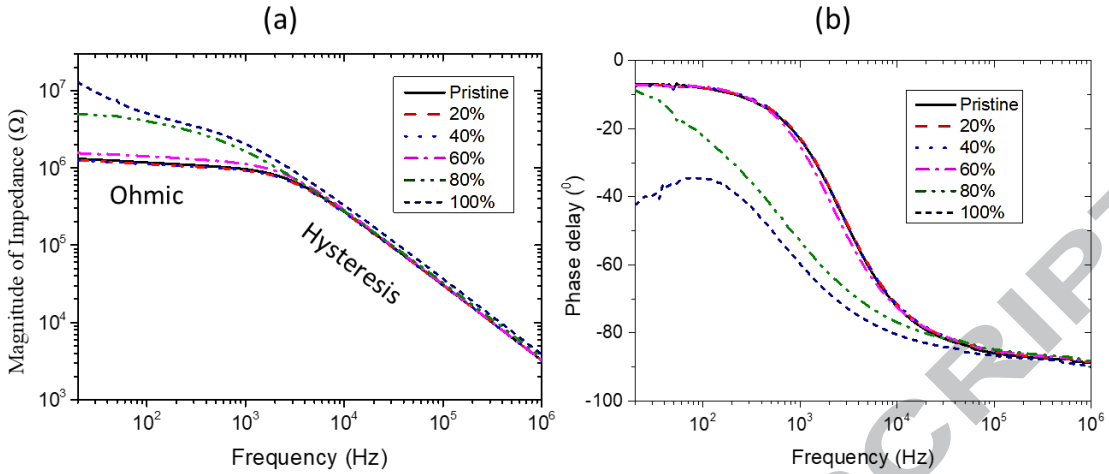

Figure 5 Bode plot of (a) impedance magnitude vs. frequency, (b) phase delay vs. frequency for all the stages of the step-loading lap shear tests

In general, when a dielectric material is subjected to an external alternating field, its dipoles are forced to orient to the direction of that field. With increasing frequency, these dipoles are unable to effectively follow the variations of the external field due to inertia effects. Therefore, hysteretic phenomena are induced, manifested as a phase delay between the excitation and the response signals.

On the other hand, damage initiation and propagation introduce a third phase, that of air, which significantly changes the dielectric properties of the interrogated system.

As can be seen from Figure 5, the magnitude of impedance and the phase delay of the single lap joints remained unaltered after subjecting the specimens up to 60% of their MSS. This behavior indicated that the level of applied stress was not sufficient to create any damage within the bondline. However, after applying a stress corresponding to 80% of the MSS, the impedance magnitude and the phase delay showed significant changes. In detail, the impedance magnitude at low frequencies (20 Hz) exhibited a significant increase from 1.55MΩ (Pristine) to 4.90MΩ (80% of MSS) and the shape of the phase delay versus frequency curves changed completely at intermediate frequencies. This behaviour can be attributed to induced damage in the nanomodified adhesive. As stated, damage induces a third phase which involves the creation of pockets of trapped air (voids) in the adhesive that disrupt the conductive CNT network and inevitably enhances the effect of interfacial polarization [34, 36]. This mechanism takes place at the interphase between two regions with different electrical properties and is reflected in the Bode plots by a reduction of the transition frequency from Ohmic to hysteretic behavior [38].

Significant changes can also be spotted in the Nyquist plot of the imaginary (Z'') versus real part (Z') of the impedance (Figure 6). The shape of the curves in the experimental Nyquist plot resembles that of a typical RC circuit in parallel [39], i.e. a semicircle with a single time constant, which is indicative of a strong capacitance element. This capacitive behavior was observed to scale according to the level of damage.

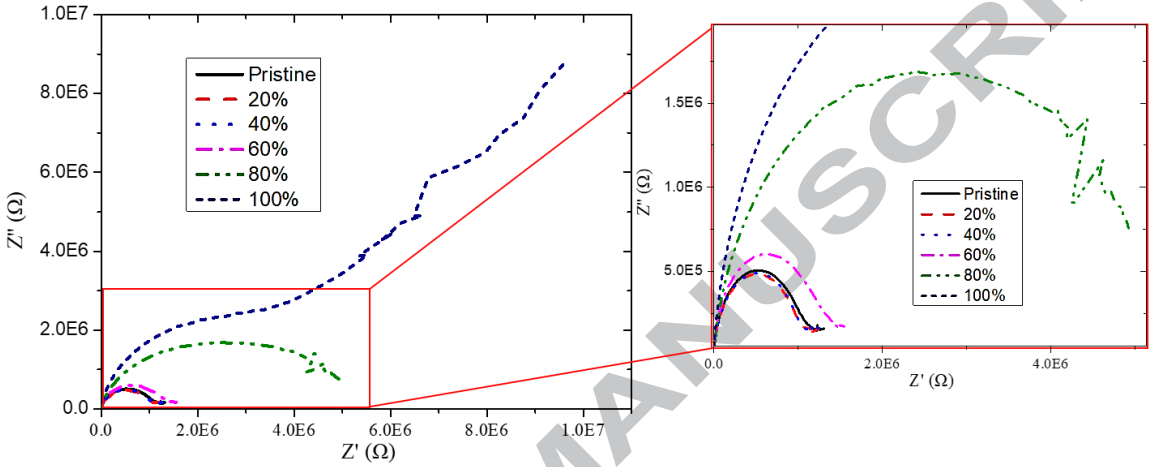

Figure 6 Nyquist plot for the pristine specimen and the specimen subjected to step-loading up to 20, 40, 60, 80 and 100% of its MSS (to better illustrate the behavior of the specimen before its fracture, a zoomed area of the Nyquist plot is depicted on the right)

The real component of the impedance at 20Hz showed a significant increase of approximately 280% reaching 4.92MΩ for the specimen that was subjected to lap shear testing up to 80% of its MSS. This quantity is directly related to the resistive character of the material and is affected by the disruption of the CNT network. On the other hand, the enhancement of interfacial polarization at the boundaries of the introduced damage, resulted in an increase in the maximum value of the imaginary part of the impedance[34, 36] Upon failure, the Z'' vs Z' curves of the specimens show completely different behavior. In this case, the curves of Nyquist plot are characterized by an abrupt increase in Z'' and Z' values while the formation of a second incomplete semi-cycle at lower frequencies denotes the failure of the single lap joint bondline.

To examine the impedance quantity that is more sensitive to the induced damage, the relative change of Z''_{max} and magnitude of impedance at 20, 100 and 1000Hz were plotted together against the percentage of MSS (Figure 7). The relative change was calculated using the impedance data of the pristine CFRP joints ($[Z-Z_0]/ Z_0= \Delta Z/ Z_0$) as a reference.

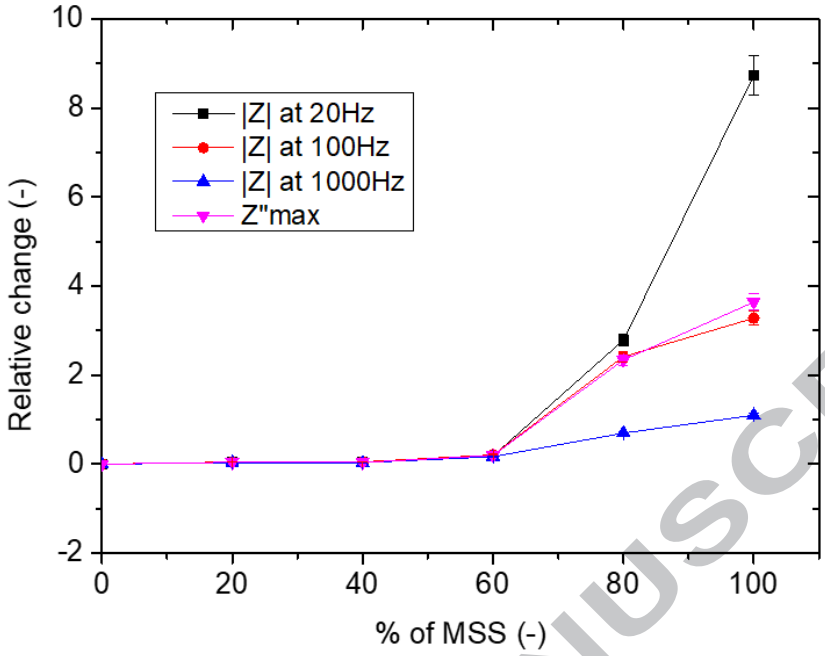

Figure 7 Relative change of the maximum value of the imaginary part of the impedance (Z''max) and magnitude of impedance (|Z|) at 20,100 and 1000Hz versus the percentage of MSS

As can be seen, |Z| at 20Hz is the most sensitive damage metric showing a significant change (approximately 300%) for the specimen that was subjected to lap shear test up to 80% of its MSS. The same quantity exhibits a second abrupt increase of approximately 900% denoting the complete failure of the single lap joint bondline. The amplitude of impedance at 100Hz and Z''_{max} show notable changes as well. The most pronounced one is for the specimen when the applied stress during the lap-shear test reaches at 80% of the MSS. A second increase to their values can be spotted after the complete failure of the bondline. Based on these results, it is evident that the developed interdigital sensor can effectively identify the initiation and propagation of damage within the bondline created by mechanical loading.

The phase thermographs obtained from the single-bonded lap joints in between the step-loading stages are depicted in Figure 8. Since the integrity of the bondline was of interest, the thermography analysis focused on that area. As can be seen, no damage can be spotted in the thermographs at low levels of applied stress (up to 60%). However, after subjecting the CFRP joints to mechanical loading up to 80% of their MSS, cracks were initiated at the free ends (run-outs) of the overlap region due to the presence of stress concentrations. Induced damage is highlighted with red lines in the bottom-right thermograph of Figure 8. These observations are in agreement with the

results obtained from the impedance analysis. At this stage, the magnitude of impedance showed significant changes indicating the presence of damage at the bondline.

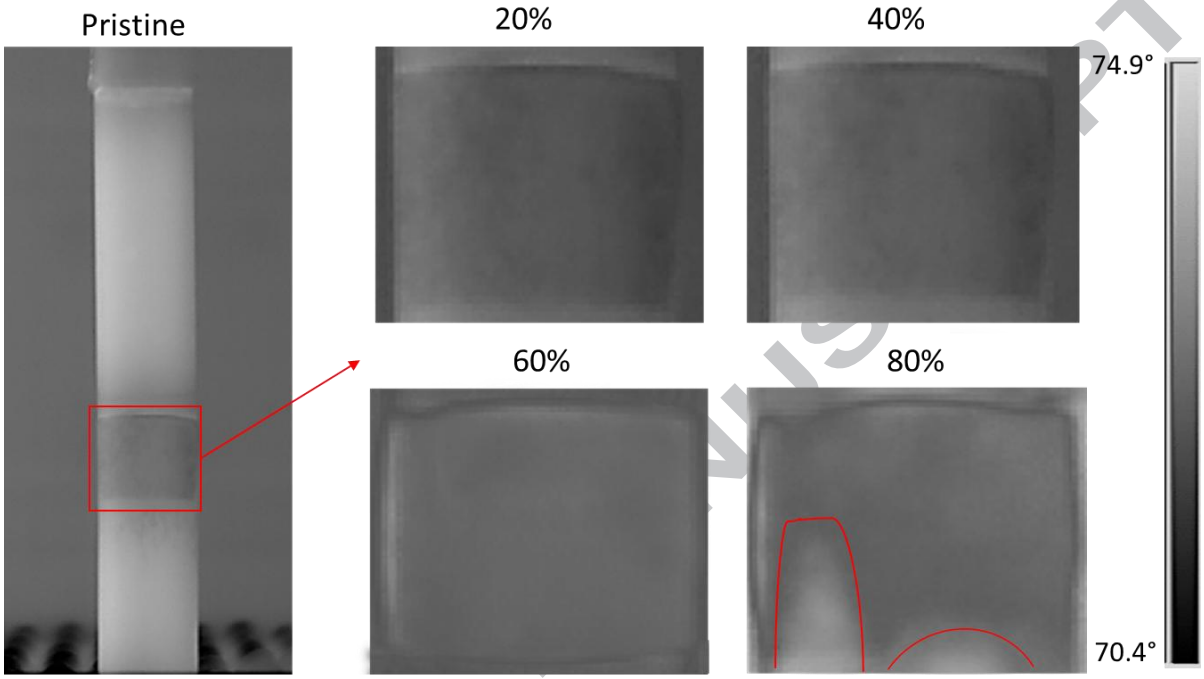

Figure 8 Phase thermographs obtained from the single-bonded lap joints in between the step-loading stages

At the end of the mechanical testing, the fracture surfaces were studied using SEM to investigate the mechanisms of failure and gain an insight of the dispersion quality of the employed filler. For that purpose, the fractured surfaces were sputter coated with gold and SEM photographs were obtained using a JEOL JSM 6510LV, Oxford Instruments scanning electron microscope. SEM images were taken from the single-lap joints with the printed interdigital sensor.

Figure 9 depicts SEM photographs taken from the single-lap joint fracture surfaces in increasing magnifications. As can be observed, the dispersion procedure broke the agglomerated MWCNTs in an efficient way, reducing the average agglomeration size and dispersing the small agglomerates throughout the bond area. The studied surface areas, indicated that the fracture was exhibited predominantly in adhesive manner between the modified epoxy and the screen-coated epoxy resin, with some portions fractured in a cohesive manner (Figure 9a-c). As seen, the studied areas comprised of islands of smooth surface, that are indicative of the fracture behaviour of an epoxy resin, mixed with areas with increased roughness that are indicative of the fracture phenomena found in epoxy nanocomposites (shear bands, filler particle pull-outs etc)

[40-42]. The modified adhesive also exhibited parallel cracks spanning the whole length of the bonded area, indicative of fracture under shear load, which could have been initiated from large sized agglomerates or defects at the edges of the specimens from the machining processes [43]. The reinforcing MWCNTs can be seen as clusters of small agglomerates with few microns of average diameter. At higher magnification, these clusters appear to comprise of a mix of mostly individual MWCNTs that interconnect smaller agglomerates (Figure 9- d). Given the fact that crack initiation indicative marks are not visible around the agglomerates, it can be postulated that the average agglomerates diameter was below the desired threshold and didn't act as crack initiation sites [44, 45].

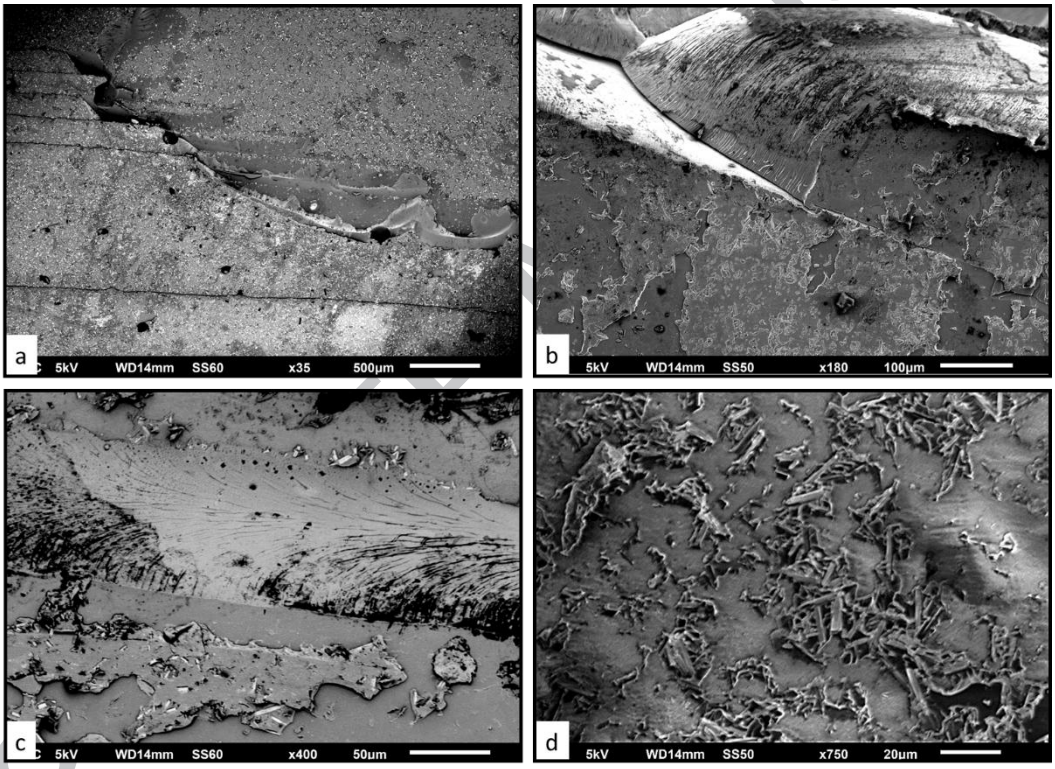

Figure 9 SEM photographs obtained from the fractured surfaces of CNT-modified single lap joints at different magnifications; (a) x35, (b) x180, (c) x400, d x750.

6 Conclusions

In the present work a novel interdigital capacitive sensor has been inkjet-printed directly onto the bondline of a single lap of a CFRP composite joint. The sensor was purposely designed to assess and evaluate the curing process as well as the structural integrity of the adhesive epoxy, by monitoring its dielectric profile. The dielectric

profile of the adhesive was monitored using one-sided impedance spectroscopy measurements over a wide frequency spectrum.

To diminish the electrode polarization effect which typically impedes the impedance spectroscopy measurements, the adhesive epoxy was nanomodified using MWCNTs. Based on the obtained results, the incorporation of the conductive nanophase within the insulating polymeric adhesive tailored the material's electrical response towards higher frequencies of the impedance spectra where the estimation of the adhesive dielectric parameters was not affected by the presence of EP effect.

Initially, the ability of the sensor to assess the bondline quality was evaluated via monitoring the evolution of the maximum value of the imaginary part of the impedance (Z''_{max}) over the adhesive curing process. As shown, the cure process was successfully monitored while the presence of an artificial defect within the bondline of a single lap joint altered the Z''_{max}, indicating the presence of a defect created during manufacturing.

Concerning the SHM of the bondline, results indicated a direct correlation between the induced damage and the impedance parameters, which proved extremely sensitive to the changes invoked in the material structure due to mechanical loading. As shown, the magnitude of impedance was the most sensitive damage metric showing significant changes to its initial values with increasing material degradation. This behavior was attributed to the disruption of the conductive CNT-network due to the induced cracks. The conclusions derived from the impedance analysis were validated using transient infrared thermography.

It should be noted that the results from the mechanical analysis, indicated that the sensor development had a negligible effect on the maximum shear strength of the single-bonded lap joints. In addition, the versatile character of the inkjet printing enables the development of sensors with different geometries for the quality assessment and SHM of more complex bonded or repaired composite structures.

7 Acknowledgements

The research leading to these results has been part of complementary activities carried at Imperial College London to support the European JTI-CleanSky2 program under the Grant Agreement n◦ 314768 (SHERLOC).

8 References

[1] A. Parashar and P. Mertiny, "Adhesively bonded composite tubular joints: Review," *International Journal of Adhesion and Adhesives,* vol. 38, pp. 58-68, 2012.

[2] M. D. Banea and L. F. M. da Silva, "Adhesively bonded joints in composite materials: An overview," *Proceedings of the Institution of Mechanical Engineers, Part L: Journal of Materials: Design and Applications,* vol. 223, no. 1, pp. 1-18, 2016.

[3] S. Budhe, M. D. Banea, S. de Barros, and L. F. M. da Silva, "An updated review of adhesively bonded joints in composite materials," *International Journal of Adhesion and Adhesives,* vol. 72, pp. 30-42, 2017.

[4] J. J. Andrew, V. Arumugam, and C. Ramesh, "Acoustic emission characterization of local bending behavior for adhesively bonded hybrid external patch repaired glass/epoxy composite laminates," *Structural Health Monitoring,* 2018.

[5] K. M. Bak, K. KalaiChelvan, G. K. Vijayaraghavan, and B. T. N. Sridhar, "Acoustic emission wavelet transform on adhesively bonded single-lap joints of composite laminate during tensile test," *Journal of Reinforced Plastics and Composites,* vol. 32, no. 2, pp. 87-95, 2012.

[6] F. Lambinet, Z. Sharif Khodaei, and M. H. Aliabadi, "Structural Health Monitoring of Bonded Patch Repaired Composite," *Key Engineering Materials,* vol. 713, pp. 135-138

2016.

[7] F. Lambinet, Z. Sharif Khodaei, and M. Aliabadi, H. , "Smart patch repair with PVDF sensors," *Key Engineering Materials,* 2017.

[8] A. De Luca, F. Caputo, Z. Sharif Khodaei, and M. H. Aliabadi, "Damage characterization of composite plates under low velocity impact using ultrasonic guided waves," *Composites Part B: Engineering,* vol. 138, pp. 168-180, 2018.

[9] Z. Sharif-Khodaei and M. H. Aliabadi, "Assessment of delay-and-sum algorithms for damage detection in aluminium and composite plates," *Smart Materials and Structures,* vol. 23, no. 7, 2014.

[10] H. Fu, Z. S. Khodaei, and M. H. F. Aliabadi, "An Event-Triggered Energy-Efficient Wireless Structural Health Monitoring System for Impact Detection in Composite Airframes," *IEEE Internet of Things Journal,* pp. 1-1, 2018.

[11] Z. Sharif-Khodaei, M. Ghajari, and M. H. Aliabadi, "Impact Damage Detection in Composite Plates using a Self-diagnostic Electro-Mechanical Impedance-based Structural Health Monitoring System," *Journal of Multiscale Modelling,* vol. 06, no. 04, 2015.

[12] M. Schwankl, Z. Sharif-Khodaei, M. H. Aliabadi, and C. Weimer, "Electro-Mechanical Impedance Technique for Structural Health Monitoring of Composite Panels," *Key Engineering Materials,* vol. 525-526, pp. 569-572, 2012.

[13] A. R. Wilson, C. Davis, W. Baker, S. D. Moss, S. C. Galea, and R. Jones, "In situ health monitoring of bonded composite repairs using a novel fiber Bragg grating sensing arrangement," presented at the Smart Materials II, 2002.

[14] W. Baker, I. McKenzie, and R. Jones, "Development of life extension strategies for Australian military aircraft, using structural health monitoring of

composite repairs and joints," *Composite Structures,* vol. 66, no. 1-4, pp. 133-143, 2004.

[15] S. A. Grammatikos, E. Z. Kordatos, T. E. Matikas, and A. S. Paipetis, "Real-Time Debonding Monitoring of Composite Repaired Materials via Electrical, Acoustic, and Thermographic Methods," *Journal of Materials Engineering and Performance,* vol. 23, no. 1, pp. 169-180, 2013.

[16] R. Mactabi, I. D. Rosca, and S. V. Hoa, "Monitoring the integrity of adhesive joints during fatigue loading using carbon nanotubes," *Composites Science and Technology,* vol. 78, pp. 1-9, 2013.

[17] T. Augustin, J. Karsten, B. Kötter, and B. Fiedler, "Health monitoring of scarfed CFRP joints under cyclic loading via electrical resistance measurements using carbon nanotube modified adhesive films," *Composites Part A: Applied Science and Manufacturing,* vol. 105, pp. 150-155, 2018.

[18] M.-H. Kang, J.-H. Choi, and J.-H. Kweon, "Fatigue life evaluation and crack detection of the adhesive joint with carbon nanotubes," *Composite Structures,* vol. 108, pp. 417-422, 2014.

[19] D. G. Bekas, Z. Sharif Khodaei, and F. M. H. Aliabadi, "Structural Health Monitoring of Scarfed Repaired Composite Panels Using Inject-Printed Patterns," *Key Engineering Materials,* vol. 774, pp. 235-240, 2018.

[20] D. Zhao, T. Liu, M. Zhang, R. Liang, and B. Wang, "Fabrication and characterization of aerosol-jet printed strain sensors for multifunctional composite structures," *Smart Materials and Structures,* vol. 21, no. 11, 2012.

[21] F. Yin, D. Ye, C. Zhu, L. Qiu, and Y. Huang, "Stretchable, Highly Durable Ternary Nanocomposite Strain Sensor for Structural Health Monitoring of Flexible Aircraft," *Sensors (Basel),* vol. 17, no. 11, Nov 20 2017.

[22] R. J. Klein, S. Zhang, S. Dou, B. H. Jones, R. H. Colby, and J. Runt, "Modeling electrode polarization in dielectric spectroscopy: Ion mobility and mobile ion concentration of single-ion polymer electrolytes," *J Chem Phys,* vol. 124, no. 14, p. 144903, Apr 14 2006.

[23] P. B. Ishai, M. S. Talary, A. Caduff, E. Levy, and Y. Feldman, "Electrode polarization in dielectric measurements: a review," *Measurement Science and Technology,* vol. 24, no. 10, 2013.

[24] C.-H. Kim, J.-H. Choi, and J.-H. Kweon, "Defect detection in adhesive joints using the impedance method," *Composite Structures,* vol. 120, pp. 183-188, 2015.

[25] A. V. Mamishev, K. Sundara-Rajan, Y. Fumin, D. Yanqing, and M. Zahn, "Interdigital sensors and transducers," *Proceedings of the IEEE,* vol. 92, no. 5, pp. 808-845, 2004.

[26] G. Gkikas, N. M. Barkoula, and A. S. Paipetis, "Effect of dispersion conditions on the thermo-mechanical and toughness properties of multi walled carbon nanotubes-reinforced epoxy," *Composites Part B: Engineering,* vol. 43, no. 6, pp. 2697-2705, 2012.

[27] *Standard Test Method for Lap Shear Adhesion for Fiber Reinforced Plastic (FRP) Bonding*, 2001.

[28] W. Zielecki, A. Kubit, T. Trzepieciński, U. Narkiewicz, and Z. Czech, "Impact of multiwall carbon nanotubes on the fatigue strength of adhesive joints," *International Journal of Adhesion and Adhesives,* vol. 73, pp. 16-21, 2017.

[29] H.-L. Ma, Z. Jia, K.-t. Lau, X. Li, D. Hui, and S.-q. Shi, "Enhancement on mechanical strength of adhesively-bonded composite lap joints at cryogenic

environment using coiled carbon nanotubes," *Composites Part B: Engineering,* vol. 110, pp. 396-401, 2017.

[30] F. H. Gojny, M. H. G. Wichmann, U. Köpke, B. Fiedler, and K. Schulte, "Carbon nanotube-reinforced epoxy-composites: enhanced stiffness and fracture toughness at low nanotube content," *Composites Science and Technology,* vol. 64, no. 15, pp. 2363-2371, 2004.

[31] S. M. J. Razavi, M. R. Ayatollahi, A. Nemati Giv, and H. Khoramishad, "Single lap joints bonded with structural adhesives reinforced with a mixture of silica nanoparticles and multi walled carbon nanotubes," *International Journal of Adhesion and Adhesives,* vol. 80, pp. 76-86, 2018.

[32] A. A. SKORDOS and K. P. IVANA, "Determination of the Degree of Cure under Dynamic and Isothermal Curing Conditions with Electrical Impedance Spectroscopy," *Journal of Polymer Science Part B: Polymer Physics* vol. 42, pp. 146-154.

[33] D. G. Bekas, G. Gkikas, G. M. Maistros, and A. S. Paipetis, "On the use of dielectric spectroscopy for the real time assessment of the dispersion of carbon nanotubes in epoxy," *RSC Advances,* vol. 6, no. 82, pp. 78838-78845, 2016.

[34] D. G. Bekas and A. S. Paipetis, "Damage monitoring in nanoenhanced composites using impedance spectroscopy," *Composites Science and Technology,* vol. 134, pp. 96-105, 2016.

[35] K. Kalkanis *et al.*, "Experimental Control of Curing via Dielectric and Fibre Bragg Grating Sensors for Composite Patch Repairs," *Sensor Letters,* vol. 9, no. 4, pp. 1265-1272, 2011.

[36] D. G. Bekas and A. S. Paipetis, "Study of the Effect of Damage on the Electrical Impedance of Carbon Nanotube Reinforced Epoxy Nanocomposites," *Journal of Sensors,* vol. 2015, pp. 1-7, 2015.

[37] J. S. Chilles, A. F. Koutsomitopoulou, A. J. Croxford, and I. P. Bond, "Monitoring cure and detecting damage in composites with inductively coupled embedded sensors," *Composites Science and Technology,* vol. 134, pp. 81-88, 2016.

[38] A. Serghei, M. Tress, J. R. Sangoro, and F. Kremer, "Electrode polarization and charge transport at solid interfaces," *Physical Review B,* vol. 80, no. 18, 2009.

[39] E. Barsoukov and J. Macdonald, Ross, *Impedance Spectroscopy Theory, Experiment, and Applications*. 2005.

[40] U. Szeluga *et al.*, "Influence of unique structure of glassy carbon on morphology and properties of its epoxy-based binary composites and hybrid composites with carbon nanotubes," *Composites Science and Technology,* vol. 134, pp. 72-80, 2016.

[41] D. Baltzis *et al.*, "Multi-scaled carbon reinforcements in ternary epoxy composite materials: Dispersion and electrical impedance study," *Composites Science and Technology,* vol. 153, pp. 7-17, 2017.

[42] M. Salviato, M. Zappalorto, and M. Quaresimin, "Plastic shear bands and fracture toughness improvements of nanoparticle filled polymers: A multiscale analytical model," *Composites Part A: Applied Science and Manufacturing,* vol. 48, pp. 144-152, 2013.

[43] A. Nemati Giv, M. R. Ayatollahi, S. H. Ghaffari, and L. F. M. da Silva, "Effect of reinforcements at different scales on mechanical properties of epoxy adhesives and adhesive joints: a review," *The Journal of Adhesion,* vol. 94, no. 13, pp. 1082-1121, 2018.

[44] Y. Zare, "Modeling the yield strength of polymer nanocomposites based upon nanoparticle agglomeration and polymer-filler interphase," *J Colloid Interface Sci*, vol. 467, pp. 165-169, Apr 1 2016.

[45] U. A. Khashaba and I. M. R. Najjar, "Adhesive layer analysis for scarf bonded joint in CFRE composites modified with MWCNTs under tensile and fatigue loads," *Composite Structures*, vol. 184, pp. 411-427, 2018.